Near-Field Enhancement of Multipole Plasmon Resonances in Ag and Au Nanowires[†]

Ezequiel R. Encina, Eduardo M. Perassi, and Eduardo A. Coronado*

INFIQC, CLCM, Departamento de Fisicoquímica, Facultad de Ciencias Químicas, Universidad Nacional de Córdoba, Córdoba (5000) Argentina

Received: December 16, 2008; Revised Manuscript Received: February 27, 2009

In this paper, we investigate theoretically the electromagnetic field enhancement arising from excitation of silver and gold nanowires (NWs) of finite length, capable of sustaining surface plasmon resonances of different multipole order, using the Discrete Dipole Approximation (DDA). The influence of NW length on the degree of enhancement and confinement of the electromagnetic field for each surface plasmon mode is analyzed by a 3D mapping of the near field for different planes around the NW as well by calculating its variation with distance along two different directions, one parallel to and the other perpendicular to the NW axis, outside of the NW. It was found that the enhancement is still significant at relative large distances from the NW end, its decay being of much longer range than that predicted by a simple dipole approximation, especially at near-infrared wavelengths.

Introduction

Nanosized metal nanoparticles (NPs) and nanostructures are the building blocks of the emerging and promising field of Plasmonics which aims to study the properties of the collective electronic excitations in metal nanostructures, normally denoted as surface plasmons, with the purpose of controlling, manipulating, and amplifying light on the nanometer scale.[1−3] In noble metal NPs, this control is achieved by a careful selection of the illumination wavelength, which needs to be close to its surface plasmon resonance (SPR), which can be tuned by changing the size, shape, composition, and dielectric environment of the metal NP.[4−11] Molecular Plasmonics[12] make use of the dramatic change of the optical properties of molecules when they are coupled to the SPR, giving rise to enhancements of several orders of magnitude in Raman spectroscopy (SERS, surface-enhanced raman spectroscopy;[13−16] TERS, tip-enhanced raman microscopy[17−22]) or to smaller but important enhancements in fluorescence microscopy (metal-enhanced flourescence, MEF[23−26]). This enhancement could be so large (on the order of 10^{14}) that the Raman spectra of single molecules can be acquired.[27−29] These enhanced optical fields of metal NPs can be useful in a variety of applications, including plasmon (bio)sensors,[30−33] sources for nanolithography,[34] probes in scanning near-field optical microscopy (SNOM), optical imaging with subwavelength resolution in nano optics,[35−37] and so forth.

Finite length nanowires (NWs) are very useful plasmonic structures as their polarizability is strongly enhanced compared to more spherical shapes and their resonance frequencies can be tuned by changing their length (L), diameter (D), and dielectric environment. In addition, they could give rise, depending on their size and aspect ratio, to spectrally separated SPR eigenmodes of different multipolar order l.[38−40] The far-field optical properties of finite length metal NWs have been investigated by extinction measurements on large ensembles.[38,39] Recently, with the aim of rigorous electrodynamics simulations, scaling laws which relate the SPR wavelength with the NW geometry have been established, and also, a general resonance condition has been derived for finite NWs as a function of l, L, and D, in good agreement with experiments.[41−43] The assignment of the multipole order has been achieved also by direct comparison of the angular scattering patterns of a given multipole order with the corresponding pattern of the point multipole.[43] These investigations gave also a detailed comprehension of the dependence of the scattering cross sections for each multipole SPR mode for Ag and Au NWs as a function of their length and dielectric environment, which are of great importance to take into account the far-field coupling between a molecule and a plasmonic structure such as in MEF.

Recently, attention has been given to the near-field optical properties of multipole surface plasmon modes of individual NWs, and several experiments of plasmonic imaging of the near field using either SNOM[44−46] or high-resolution catholuminescence spectroscopy (HRCLS)[47] have been performed. In another series of experiments, the capabilities of higher order multipole SPR of finite NWs to produce significant SERS enhancement has also been demonstrated for NWs arrays fabricated by nanosphere lithography.[39] The possibility of a subwavelength imaging system without a lens or a mirror but with an array of metallic nanorods has also been reported recently, in which the near-field components of dipole sources were plasmonically transferred through the rod array to reproduce the source distribution on the other side.[48]

In view of the potential applications of finite NWs for SERS, TERS, plasmonic lithography, or near-field imaging, it is of great importance to account for the degree of confinement and enhancement of the electromagnetic field around this special kind of plasmonic nanostructures. In this work, we have performed rigorous electromagnetic simulations using the DDA method to study the behavior of the near-field optical properties of the several plasmon eigenmodes sustained by finite Ag and Au NWs as a function of their length and dielectric environment for a fixed diameter of 40 nm.

A key quantity in plasmon-enhanced spectroscopies is the electromagnetic field enhancement defined as $|E|^2 = (E \cdot E^*)/(E_0 \cdot E_0^*)$, where E is the complex local electromagnetic field at a given position, while E_0 is the complex incident electromag-

[†] Part of the "George C. Schatz Festschrift".

* To whom correspondence should be addressed. E-mail: coronado@fcq.unc.edu.ar.

10.1021/jp811089a CCC: $40.75
Published on Web 03/16/2009

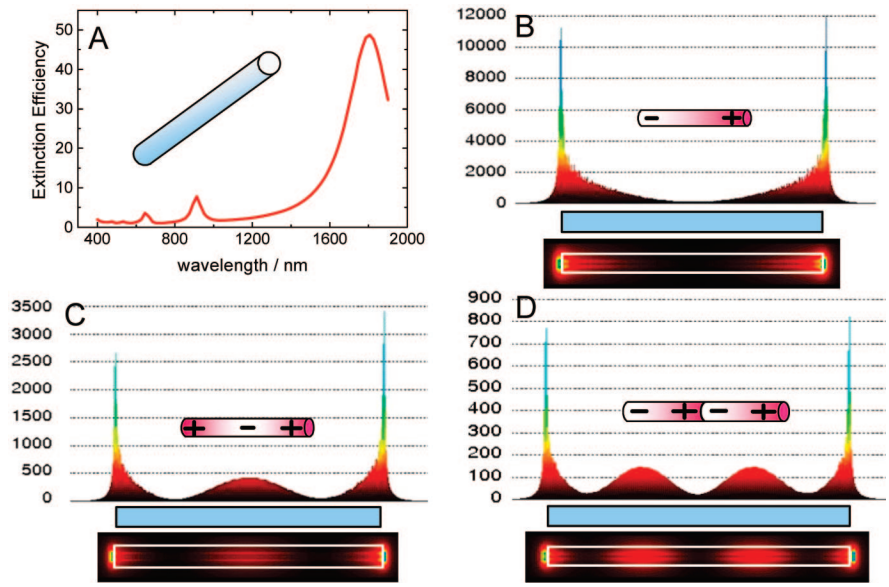

Figure 1. (A) Averaged extinction spectrum for a Ag NW ($L = 480$ nm, $D = 40$ nm) in vacuum; the various peaks correspond to different multipole plasmon resonances. (B−D) $|E|^2$ values on a plane parallel to the long symmetry axis located on the top at 1.6 nm above the NW for the (B) dipole, (C) quadrupole, and (D) octupole mode. In each of the figures, the central gray rectangle schematically represents the NW, while the upper and lower panels show a lateral and top view of $|E|^2$, respectively.

netic field. According to the electromagnetic mechanism, the amplification of the Raman intensity for TERS and SERS is proportional to the square of the enhancement, as has been shown in several works.[9,13−16,22,49]

We illustrate the general near-field patterns of the different eigenmodes by performing a 3D mapping of its enhancement for a particular NW on selected planes perpendicular and parallel to the NW long axis in order to characterize the near-field intensity imagines for the different eigenmodes. For each particular eigenmode and length, we have studied the maximum field enhancement, which can be achievable at some particular location near the NW surface, the surface average field enhancement, and the variation of the field enhancement with distance along two directions, one parallel and the other perpendicular to the NW axis, both starting from the point of maximum field enhancement. These directions were chosen because of the relevance to determine the long-range distance dependence of SERS and TERS.

Methodology

All of the calculations were performed using the DDA approach. The details of this method have been published in several places.[50,51] Briefly, one represents the particle by a cubic lattice of point dipoles, each of which is assumed to have a polarizability that is determined by the dielectric constant associated with the material. If there are N dipoles whose positions and polarizabilities are denoted by r_i and α_i, then the induced dipole moment P_i in each dipole in the presence of an applied linearly polarized plane wave field is $P_i = \alpha_i E_{\mathrm{loc},i}$ ($i = 1, 2, ..., N$), where the local field $E_{\mathrm{loc}}(r_i)$ is the sum of the incident and retarded fields of the other $N - 1$ dipoles. In all of the calculations, we have used a constant grid spacing of 1.6 nm. The calculations were performed for Ag and Au NWs with a constant diameter (40 nm) and various lengths from 40 to 800 nm, while the dielectric functions for each noble metal where taken from Palik.[52] In order to calculate $|E|^2$, probe dipoles with almost zero polarizability were added outside of the target in such a way that their presence did not produce any perturbation on the system.

Results and Discussion

Mapping the Near-Field Enhancement of SPR. In this section, we will give the general features of the near-field patterns of the multipole longitudinal SPR modes by analyzing a Ag NW of $L = 480$ nm. We have chosen this particular length because from all of the NWs analyzed in this work, it is the longest one capable of sustaining three SPRs of different order in the spectral range where experimental values of the dielectric constant for Ag and Au are available; in this way, a comparison between various multipole orders can be performed (longer NWs were also analyzed, but their dipole SPRs peak at frequencies outside of this range). This NW shows on its averaged extinction spectrum three peaks corresponding to the dipole ($l = 1$), quadrupole ($l = 2$), and octupole ($l = 3$) modes, as depicted in Figure 1A. As the position of the resonance wavelength for each plasmon mode does not change with the NW orientation with respect to the incident electric field and as it is our purpose to investigate the "on resonance" near-field response, we will discuss the enhancement of the electromagnetic field for this NW excited with longitudinal polarization for the odd plasmon modes and for excitation at 45° between the incident electric field and the nanowire major axis for the quadrupole plasmon mode (as this even mode could not be excited with longitudinal polarization due to symmetry considerations). Figure 1B−D shows $|E|^2$ for these modes on a plane parallel to the long symmetry axis located on the top at 1.6 nm above the NW. In each of these figures, the central gray rectangle schematically represents the NW, while the upper and lower panels show a lateral and top view of $|E|^2$, respectively. Independently of the multipole order, the maximum $|E|^2$ is achieved at the NW ends, while the quadrupole and the octupole modes depict, in addition, one and two beats along the major axis, respectively. For $l = 2$, the beats have a maximum $|E|^2$ value at $L/2$, while for $l = 3$ the two beats reaches their maximum values at $L/4$ and $3L/4$, respectively, their intensities being around 6 times smaller than the values reached at the NW end. These results are in agreement with recent near-field pattern images of Au NWs measured using different techniques.[44−47]

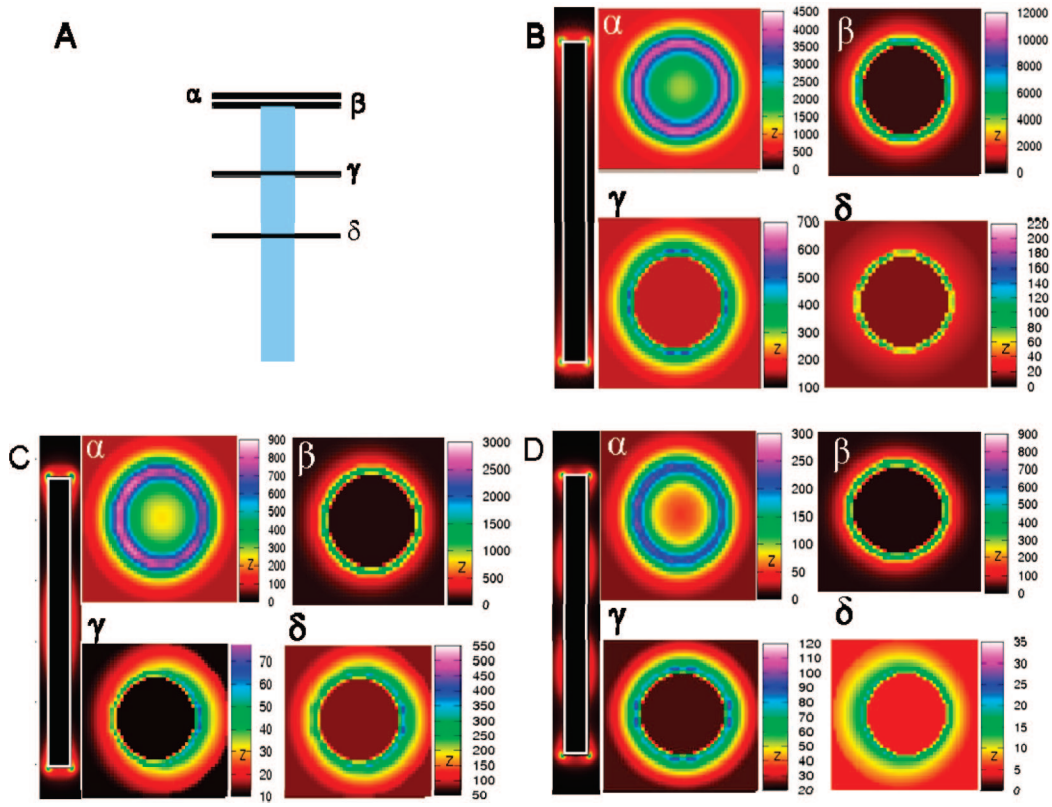

Figure 2. (A) Scheme of the planes α, β, χ, and δ perpendicular to the Ag NW axis (L = 480 nm, D = 40 nm), where the $|E|^2$ distributions are shown. Cross-sectional distributions of $|E|^2$ on planes α, β, χ, and δ for the (B) dipole, (C) quadrupole, and (D) octupole mode.

The cross-sectional distribution of $|E|^2$ on selected planes perpendicular to the NW major axis indicated in Figure 2A are shown in Figure 2B−D for each plasmon mode. Although the maximum values of $|E|^2$ for planes α and β vary according to the multipole order, the enhancement pattern is almost the same for all modes, except from some slight differences that will be described below. For plane α, at 3.2 nm outside of the NW, this pattern consists of a central spot surrounded by several rings of different intensities. Moving on this plane from the central spot along the radial direction, $|E|^2$ increases monotonically until some critical value, and then, it starts to decrease. Quite interesting, for $l = 2$, $|E|^2$ is not symmetric around the perimeter, being more intense on one side than on the opposite one (Figure 2C); this feature is also present for this mode in all of the other planes. A possible explanation for this behavior is provided by a detailed analysis of the charge distribution of the field around the perimeter of the NW, which indicates that for each transverse plane, the sign of the charge is the same all around the NW perimeter. This fact implies that the asymmetry observed is not due to opposite charges located within a given plane but to a nonuniform distribution of charges of the same sign. This is exemplified in the vector plot performed, for instance, for planes β and δ, where the magnitude and direction of the field is shown (see Figure 1 in Supporting Information). This asymmetry on the charge distribution should be compensated on another plane where an opposite polarization charge is developed, that is, if in plane δ more negative charge density is accumulated on the left side, on plane β, more positive charge density must be accumulated on the right side.

When considering plane β, that is, just at the NW edge, a different distribution is obtained; $|E|^2$ is very low within the NW geometrical cross section but has a ring of maximum value just around its perimeter, beyond which it decreases along the NW radial direction. Another two planes of interest are those along the NW where $|E|^2$ shows additional peaks or minima as planes γ and δ. For the dipole mode, it is interesting to note that the enhancement around plane γ is greater than that produced by any of the other two modes with a peak value of around 400−500, almost 4 and 7 times greater than the values calculated for the octupole ($|E|^2 = 90$) and quadrupole ($|E|^2 = 60$). This feature of the dipole mode indicates that the great enhancement value (around 8000) at the end of the NW decays at a rate small enough to surpass the values corresponding to the $l = 2$ and 3 modes. Note also that the enhancement factor for the even mode, which has a minimum at this position, is only slighter smaller than the octupole (where there is a maximum of $|E|^2$), a fact that also points out that although the enhancement is not uniform along the NW axis, it could be significant even at the "node" positions. The distribution of $|E|^2$ observed by slicing through plane δ depicts the highest values for the even mode followed by the $l = 1$ and 3 modes. In this case, although the dipole mode has its smallest value along the axis on this plane, it is only 4 times smaller compared with the $l = 2$ mode, which emphasizes again the feature mentioned above; the field never vanishes along the NW major axis. Indeed, this minimum value of $|E|^2$ for the dipole is still 6 −7 times greater than that of the octupole (where there is a minimum). Summarizing this section, it can be stated that for NWs illuminated on resonance with their respective SPR modes, the regions making the major contribution to the enhancement are located at the NW ends for all of the modes and that the decay of the field along the major axis never vanishes. The regions around the beats observed for the higher order multipoles can give rise, depending on the plane and excited mode, to enhancements even smaller than those produced by the dipole mode.

The Effect of NW Length on the Magnitude and Distance Dependence of $|E|^2$. As analyzed in the above section, the greatest enhancements are achieved, for all of the SPR modes,

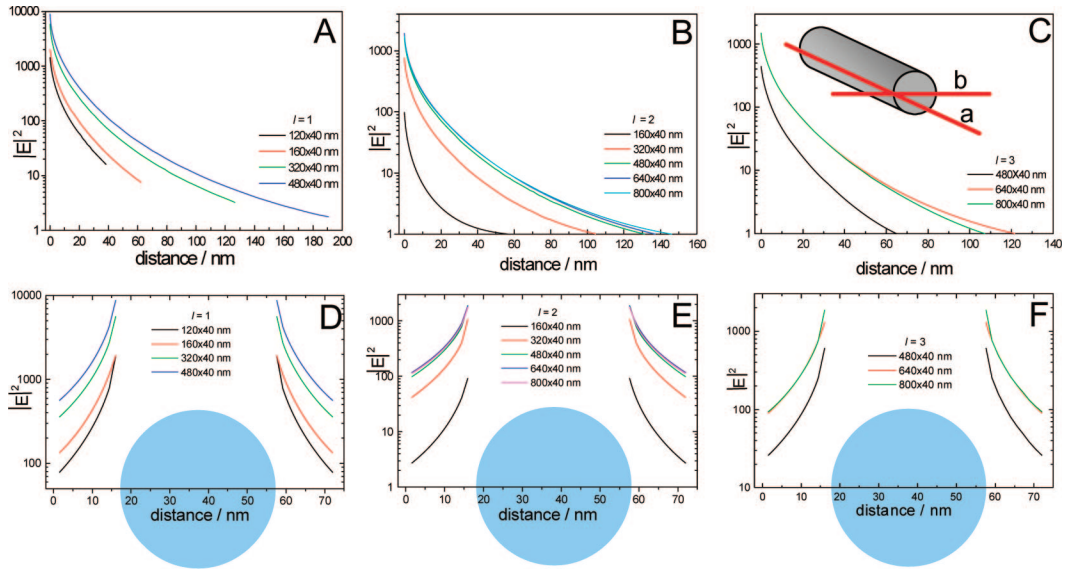

Figure 3. Variation of $|E|^2$ with distance along direction a for the (A) dipole, (B) quadrupole, and (C) octupole mode for Ag NWs of different lengths excited at their respective resonance wavelengths. Variation of $|E|^2$ with distance along direction b for the (D) dipole, (E) quadrupole, and (F) octupole mode for Ag NWs of different lengths excited at their respective resonance wavelengths. The inset in (C) schematically depicts the directions a and b.

near the NW ends. Importantly, for direct plasmon sensing as well as for SERS, TERS, or near-field imaging applications, it is of great interest to study the variation of $|E|^2$ outside of the NW surface. The effect of length on the near-field enhancement for noble metal nanorods with convex ends has been recently studied by Aizpurua et al.,[53,54] specially focusing on the dipole plasmon mode and a particular distance (1 nm) from the nanorod using the boundary element method. Related work based on antenna theory has been performed by Novotny.[55] However, at present, the distance dependence of the enhancement as well as its variation with the multipole order are issues which still remain to be addressed. Therefore, in this section, we will analyze the magnitude of the near-field enhancement and its decay with distance along two directions, one starting at one point of maximum $|E|^2$ parallel to the major axis (this initial point is located around the NW perimeter on plane β of Figure 2), which will be denoted as direction "a", and the other starting on the same point but perpendicular to the major axis, which will be denoted as direction "b". Panels A−C and D−F of Figure 3 show the variation of $|E|^2$ for different multipole orders along directions a and b, respectively, for Ag NWs of different lengths excited at the respective resonance wavelengths (see Table 1). In general, whatever the multipole order and for both directions, the enhancement is greater as the length is increased. This effect is more pronounced for the dipole mode, as the maximum enhancement at the NW end increases almost 200 (for Au) or 40 times (for Ag) at the NW end when the length varies from from 40 to 480 nm. There are several factors that may contribute to these results; for the same multipole order and the same noble metal, as the length is increased, the plasmon resonance red shifts with respect to interband transition, a more electron-free behavior, and therefore produces an increment of the enhancement. However, radiation damping effects, which increase with NW length, could reduce the enhancement after some critical length, depending on the mode (see Table 1).

Excluding the spectral range near the interband transitions, the variation with length of the maximum enhancement at the NW end is less pronounced for the higher order modes, as their SPR wavelengths have a smaller red shift with increasing length, compared with that of the dipole SPR.[42]

TABLE 1: Maximum Enhancement Factors $|E|^2_{max}$ and Surface Average Enhancement Factors $|E|^2_{avg}$ for Different Multipole Orders (l) of Ag and Au NWs at the Corresponding Resonance Wavelength, λ_{res}[a]

metal	length/nm	l	λ_{res}/nm	$\lvert E\rvert^2_{avg}$	$\lvert E\rvert^2_{max}$	$-\varepsilon'$	ε''	Q
Ag	40	1	415	95	290	4.5	0.75	
Ag	120	1	650	318	1913	28.4	1.15	
Ag	160	1	761	430	1936	48.3	1.44	8.7
Ag	320	1	1291	700	5600	78.2	6.20	7.7
Ag	480	1	1805	860	8200	157.7	19.40	
Ag	160	2	459	29	96	6.5	0.73	
Ag	320	2	680	143	1060	19.1	1.22	
Ag	480	2	912	229	1890	37.7	2.16	
Ag	640	2	1148	221	1875	61.1	4.00	
Ag	800	2	1384	196	1760	90.9	7.58	
Ag	480	3	647	77	600	16.8	1.14	16.7
Ag	640	3	803	194	1270	28.2	1.51	22.2
Ag	800	3	951	167	1850	41.0	2.50	18.2
Au	40	1	537	15	47	4.4	2.38	
Au	120	1	695	318	2146	16.0	1.04	
Au	160	1	800	436	2124	23.9	1.50	10.2
Au	320	1	1321	647	5271	79.7	7.10	8.3
Au	480	1	1795	873	8830	159.0	19.00	9.7
Au	160	2	495	3	4	2.4	3.46	
Au	320	2	722	143	1011	17.9	1.12	
Au	480	2	940	204	1240	36.0	2.34	
Au	640	2	1163	178	1490	59.4	5.90	
Au	800	2	1390	180	1609	89.6	8.12	
Au	480	3	703	110	840	16.6	1.06	18.1
Au	640	3	837	163	1070	27.0	1.67	20.5
Au	800	3	982	60	1850	39.8	2.76	17.4

[a] The real ε' and imaginary ε'' parts of the noble metal dielectric function at each SPR are given along with same selective values of the quality factors Q.

Let us now compare the lengths of the NWs needed to excite a given SPR mode at the same wavelength and their respective enhancements. For example, at a wavelength $\lambda = 650$ nm, it is possible to excite on resonance the $l = 1$, 2, and 3 modes if the NW lengths are 120, 320, and 480 nm, respectively, producing maximum $|E|^2$ values of around 2000, 1000, and 600, respectively. Considering that we are at the same wavelength, the small enhancement of the higher order modes is due to the larger NW size, which will produce more damping. If we now choose a higher wavelength in order to produce more enhancement, for instance, $\lambda = 1100$ nm, the respective NW lengths could be

estimated to be 250, 620, and 980 nm, giving enhancements of 5000, 2000, and 1500, so that the most favored is always the dipole mode, which is always the one subject to less radiation damping.

As mentioned above for SERS or TERS, it is of great importance to know not only the magnitude of the maximum enhancement but also its long-range dependence, that is, its variation with distance. The SERS distance dependence is critical from both the mechanistic as well as the practical point of view. The electromagnetic mechanism predicts that neither TERS nor SERS requires the adsorbate to be in direct contact with the surface but within a certain sensing region. Also, for many practical applications, it is not possible to have a direct contact between the adsorbate of interest and the surface because the surface is modified with a capture layer (such as in biological detection) for specificity or biocompatibility.[7] As far as we know, there are only a few sets of experiments where the SERS distance dependence has been measured.[16] These experiments have been performed around small metal spheres and in a limited distance range. Because the field should decay with r^{-3} in this case (where r is the distance from the sphere center to the observation point), using the $|E|^4$ approximation, the overall distance dependence of the enhancement will scale with r^{-12}. The experimental SERS distance dependence was found to be fitted quite well with the following expression

$$\frac{I}{I_0} = \left(1 + \frac{r}{a}\right)^{-10} \quad (1)$$

where I/I_0 is the normalized intensity of the Raman mode and a is the averaged size of the field enhancement features on the surface. The exponent has been modified to -10 to take into account that the sensing area increases with r^2. Not considering this surface effect, the normalized field enhancement (whose square will give the SERS enhancement) should follow the following law for a dipole field of a small sphere

$$\frac{I}{I_0} = \left(1 + \frac{r}{a}\right)^{-6} \quad (2)$$

In order to make a comparison with eq 2, in Figure 4, we have plotted the normalized decay ($|E|^2/|E|^2_{max}$) of the enhancement along direction "a" for all of the NWs plasmon modes and lengths. Quite surprisingly, the normalized enhancements collapse to a single curve, independently of the plasmon mode and multipole order. In order to give physical insight into the nature of this long-range distance dependence, we have compared it with the decay of a dipole field. From the comparison, it results that the decay of the enhancement can not be properly described by a dipole field in the whole distance range. In fact, eq 2 (with $a = 18$ nm) gives a roughly good fitting at small distances (5−6 nm), but for larger distances, the present calculations show a decay of much longer range than that predicted for a dipole field. Interestingly, we found, after many trial functions, that the following empirical triple exponential decay function does a very good job of accounting for the distance dependence of the normalized enhancement in the entire distance range

$$\frac{|E|^2}{|E|^2_{max}} = A_1 \exp(-x/d_1) + A_2 \exp(-x/d_2) + A_3 \exp(-x/d_3) \quad (3)$$

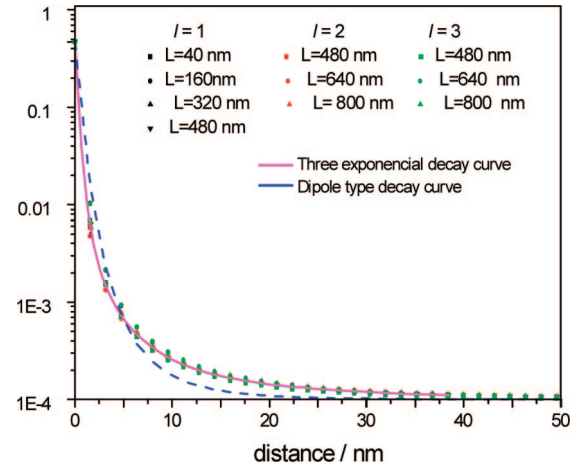

Figure 4. Variation of the normalized enhancement factor along direction a for Ag NWs of different lengths and plasmon order l. The solid lines correspond to fitting the averaged normalized data to a three exponential function (red —) and to a dipole decay function (blue —).

with $A_1 = 0.42$, $d_1 = 3.7$ nm; $A_2 = 0.41$, $d_2 = 0.93$ nm; and $A_3 = 0.172$, $d_3 = 14.3$ nm. It should be very interesting to test the above theoretical results by performing experiments covering a long distance range from the tip, especially at near-infrared wavelengths on resonance with the SPR mode. At variance with decay in direction a, the normalized enhancement along direction b does not converge to the same curve for all of the SPR eigenmodes and lengths.

The Dependence of $|E|^2$ on the Multipole Order. For the same NW dimensions and the same noble metal, the enhancement increases as the multipole order is decreased. For example, for the three SPRs sustained by the 480 nm length Au NW, the maximum enhancement of the dipole resonance is almost 3 times greater than that produced by the $l = 2$ SPR, which in turn is a factor of 4 greater than the largest enhancement produced by the $l = 3$ SPR. These trends can be explained considering that the $l = 1$, 2, and 3 resonances peak. respectively. at 1795, 940, and 703 nm, that is, the SPR mode that is more red shifted produces a larger enhancement. This is the dominant effect, despite the fact that the imaginary part of the dielectric constant, ε'', is greater for the dipole mode ($\varepsilon'' = 19$) than for the other two modes $\varepsilon'' = 2.34$ and 1.06, which will cause more damping, as evidenced by the quality factor, Q, calculated from the extinction spectra ($Q = 9.7$ for $l = 1$ and $Q = 15.2$ for $l = 3$). This leads to the conclusion that care must be taken when considering only the Q factor as a figure of merit to account for the electromagnetic field enhancement since there are two competing processes which would determine the enhancement value, the magnitude of the red shift as well as the damping mechanism. In this case, it seems that the first effect is much more important than the second.

Influence of the Dielectric Environment. In Figure 5, we show the values of $|E|^2$ along direction b for a Ag NW ($L = 240$ nm) placed in three different dielectric environments corresponding to vacuum ($\varepsilon_0 = 1$), water ($\varepsilon_0 = 1.77$), and ITO ($\varepsilon_0 = 2.7$). For $l = 1$ (Figure 5A), the maximum value of $|E|^2$ decreases with ε_0, while an opposite trend is found for $l = 2$. This result seems to be difficult to explain as it has been suggested that the surrounding media behaves as a screen which always reduces the field enhancement. As there are not analytical expressions to compute the field enhancement for cylindrical NWs, in order to understand this puzzle, we will use the exact solution of Laplace's equation for a prolate spheroidal particle,

whose shape can be regarded as close to that of the cylinders considered in this work. In this approximation, the expression for the enhancement as a function of location on the surface is given by[56,57]

$$|E|^2 = |1 - g|^2 + \frac{[2\,Re[(1-g)(g)^*]]\eta^2}{Q_1(\xi_0^2)(\xi_0^2 - \eta^2)} + \frac{|g|^2\eta^2}{Q_1^2(\xi_0)(\xi_0^2 - 1)(\xi_0^2 - \eta^2)} \quad (4)$$

where $Q_1(\xi_0)$ and ξ_0 are geometrical factors defined as

$$Q_1(\xi_0) = \frac{1}{2}\xi_0 \ln\left(\frac{\xi_0 + 1}{\xi_0 - 1}\right) - 1 \qquad \xi_0 = (1 - AR)^{-1/2} \quad (5)$$

with AR as the ratio between the minor and the major axis. In eq 4, η specifies the position over the surface in spheroidal coordinates where the field is going to be computed, which is related to the usual spherical coordinate θ via

$$\eta = \cos\theta\left(\frac{\xi_0^2 - 1}{\xi_0^2 - \cos^2\theta}\right) \quad (6)$$

The factor g is given by

$$g = \frac{\varepsilon - \varepsilon_0}{\varepsilon + \chi\varepsilon_0} \quad (7)$$

$\varepsilon = \varepsilon' + i\varepsilon''$ is the complex dielectric function of the metal, ε_0 denotes the dielectric constant of the medium, and χ is a geometrical factor that depends on AR (see ref 56). On resonance, $\varepsilon' = -\chi\varepsilon_0$, so that the factor g can be expressed as

$$g = 1 + \left(\frac{\varepsilon_0 - \varepsilon'}{\varepsilon''}\right)i \quad (8)$$

Substituting eq 8 into eq 4 and after a few arrangements, we obtain the following expression for the on resonance enhancement factor for a prolate spheroid

$$|E|^2 = \left(\frac{\varepsilon' - \varepsilon_0}{\varepsilon''}\right)^2\left[1 + \frac{2\eta^2}{Q_1(\xi_0^2)(\xi_0^2 - \eta^2)} + \frac{\eta^2}{Q_1^2(\xi_0)(\xi_0^2 - 1)(\xi_0^2 - \eta^2)} + \frac{\eta^2(\varepsilon'')^2}{Q_1^2(\xi_0)(\xi_0^2 - 1)(\xi_0^2 - \eta^2)(\varepsilon' - \varepsilon_0)^2}\right] \quad (9)$$

As the factor in brackets depends mainly on geometry (the fourth term of this factor has a negligible contribution to the sum compared to the other three terms), for two NWs of exactly the same geometry, the enhancement should be controlled by the first factor. Hereafter, this factor, that is, $((\varepsilon' - \varepsilon_0)/\varepsilon'')^2$, will be denoted as R_d^2.

Now, with the aim of eq 9, we will try to explain the different behavior observed for the two modes just by analyzing the variation of R_d when the medium is changed, taking into account the values of ε' and ε'' at their respective resonance wavelength on each media. The factor in brackets is not expected to be modified as long as the geometry is the same. The R_d factors computed using the data for the dielectric constants for each SPR wavelength and each mode for the 240 nm length Ag NW are shown in Table 2. An excellent correspondence between the trends followed by the enhancement factor for both modes ($l = 1$ and 2) as the dielectric media is changed and the respective trends followed by the R_d values has been obtained.

These values must be taken with care, as a trend, not as a figure of merit to quantify the absolute enhancements, but they should be very helpful if one whishes to compare the relative enhancements of NWs of the same size and shape but in different dielectric environments or, as we will see in the next section, to compare the relative enhancement of NWs of different noble metals but with the same size and shape in the same dielectric environment.

The Nature of the Noble Metal. As it is has been documented for many nanostructures, at visible frequencies, silver is more efficient than gold in producing electromagnetic field enhancement.[56−58] However, when considering two NWs of the same dimensions, one of Ag and the other of Au, depending on the multipole order and wavelength at which these resonances are produced, in some cases, the opposite trend could be obtained. For small lengths, Au is the least efficient as its resonance wavelength is very near its interband transition. For instance, for NWs with $L = 40$ nm, the dipole enhancement is 6 times smaller for Au than that for Ag, while for $L = 120$ nm,

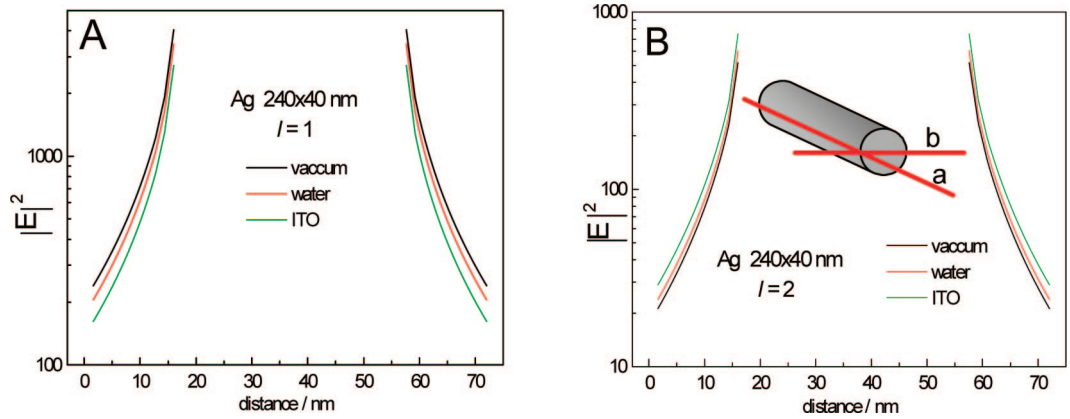

Figure 5. Influence of the dielectric environment on the magnitude and decay of the near-field enhancement along direction b for a Ag NW (L = 240 and 40 nm) excited at the respective resonance wavelengths for the (A) dipole mode and (B) quadrupole mode. The inset in (B) schematically depicts the directions a and b.

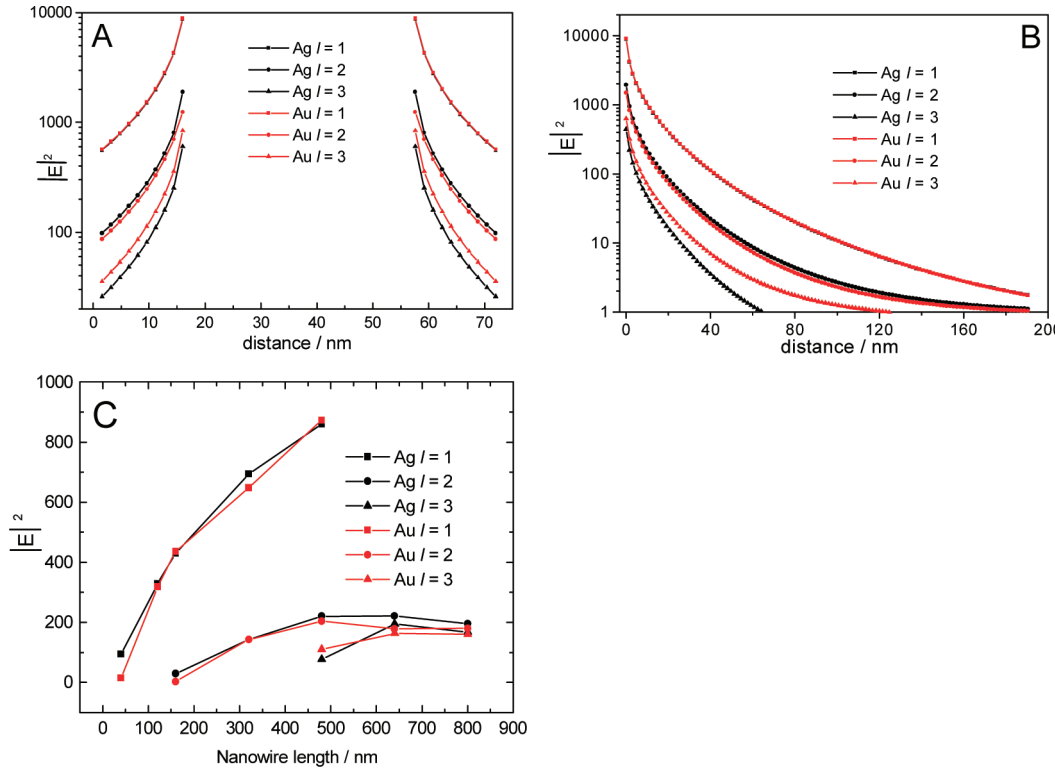

Figure 6. Comparison of the variation of $|E|^2$ with distance along (A) direction a and (B) direction b between Ag and Au NWs with the same dimensions ($L = 480$ nm) for $l = 1$, 2, and 3 modes excited at their respective resonance wavelengths. (C) Surface averaged values of $|E|^2_{avg}$ for Ag and Au NWs of different lengths for $l = 1$, 2, and 3 modes.

TABLE 2: Correlation between the Factor R_d and the Electromagnetic Field Enhancement for the $l = 1$ and 2 modes for a Ag NW with $L = 240$ nm in different dielectric environments[a]

l	medium	ε_0	$-\varepsilon'$	ε''	R_d	λ_{res}/nm	$\lvert E\rvert^2_{max}$
1	vacuum	1	48.29	3.12	15.8	1028	4046
1	H_20	1.77	87.54	7.19	12.4	1360	3463
1	ITO	2.69	133.98	14.75	9.3	1666	2730
2	vacuum	1	12.25	0.83	16.0	570	516
2	H_20	1.77	22.15	1.39	17.2	725	601
2	ITO	2.69	34.45	1.86	20.0	875	753

[a] The values of the dielectric constant of the medium (ε_0) and the real and imaginary part of the dielectric constant of Ag (ε' and ε'') at each resonance wavelength (λ_{res}) are also indicated in each column.

the enhancement produced by both metals is almost the same (see Table 1). A dramatic difference is observed when comparing the quadrupole enhancement produced by a Ag and Au NW with $L = 160$ nm because, in this case, the Au quadrupole resonance wavelength is very close to its interband transition, in such a way that the enhancement produced by Au is very small, being almost 20 times smaller than that produced by a Ag NW. For NWs illuminated at wavelengths beyond 680 nm, there are not any significant differences in the enhancement factors produced by Ag or Au NRs for any nth pole order (see Table 1). This fact is more evident for $l = 1$, as the resonance wavelength for this mode lies on the near-IR region where there are almost no differences between the ε values for both metals.

Figure 6 shows a comparison of the long distance dependence of $|E|^2$ along directions a (Figure 6A) and b (Figure 6B) for Ag and Au NWs of the same dimensions ($L = 480$ nm) for different l values. For both directions and for both metals, there is no significant difference in the $|E|^2$ distance decays for the $l = 1$ and 2 modes (Ag being a little more efficient than Au for $l = 2$). However, for $l = 3$, the $|E|^2$ values along both directions are greater for Au than those for Ag. The first result is almost evident as there are not any differences in the dielectric constants in the resonance wavelengths for the dipole mode. The different enhancements observed for the other two modes can be rationalize on the same ground as the analysis performed in the previous section, that is, the factor R_d can be used as a figure of merit to compare relative enhancements of two NWs of different metals, having the same dimensions, in the same dielectric environment, for the same multipole order. The values of R_d for Ag are 17.9 for $l = 2$ and 15.6 for $l = 3$, while for Au, they are 15.8 for $l = 2$ and 16.6 for $l = 3$, following the same trend as the corresponding enhancement shown in Table 1.

Let us finally discuss the surface average field enhancement produced by Ag and Au NWs of different lengths, a quantity that is of great interest for SERS experiments measuring the enhancement produced by the collective response of a monolayer of molecules around a NW. These values were calculated by averaging all of the enhancements computed at a distance of 1.6 nm from the whole NW surface. The results of our calculations are shown in Table 1 and plotted in Figure 6C for each noble metal, length, and plasmon mode. In agreement with previous studies performed for prolate NPs, the surface average is, depending on the mode excited, around 4−10 times smaller than the maximum field enhancement.[56] It should be noticed that, except for the dipole plasmon mode, this average enhancement does not follow the same trend as $|E|^2_{max}$ as the NW length is increased. For example, $|E|^2_{avg}$ for the $l = 3$ mode first increases and then decreases with length (in the range from $L = 480$ to 800 nm), while $|E|^2_{max}$ always increases in this length range. This effect is due to the fact the increment on $|E|^2_{max}$ at the tip of the NW is not compensated by the modest increment produced on the beats (see the discussion about the near-field patterns

produced by each plasmon mode) when the length is increased and also because the enhancement values are averaged over a larger surface area.

As a final remark, note that there is a very good correspondence between the R_d values and the corresponding enhancement ($|E|^2_{max}$ or $|E|^2_{avg}$) when comparing NWs of different metals but with the same length and for the same multipole order. For example, for the $l = 3$ mode, the R_d values computed for equal length ($L = 640$ nm) Au and Ag NWs in vacuum are 16.8 and 19.3, respectively, in very good correspondence with the values of $|E|^2_{avg}$ and $|E|^2_{max}$, which are, respectively, 163 and 1070 for Au and 194 and 1270 for Ag.

Conclusions

A 3D mapping of the near-field enhancement produced "on resonace" by Ag and Au NWs revels that, whatever the multipole order, the maximum field enhancement is produced at the NW ends. Higher order multipoles present a number of beats of $|E|^2$ along the major axis, with intensities lower than those produced at the NW ends but with significant values, especially at near-infrared wavelengths, a fact that is in agreement with recent experiments where the near field has been mapped. The enhancement shows the most significant variation with NW length for the dipole mode, as it is the one which experiences a more pronounced red shift. For higher order modes, $|E|^2$ increases with length at a lower rate than the dipole and reaches a plateau or displays a slight decrease after some critical value. The long-range distance dependence of $|E|^2$ was found to be of much longer range than that of a simple dipole field. For a direction parallel to the NW axis, the distance dependence of the normalized enhancement is almost the same as that for Ag NWs of different lengths and multipole order and could be fitted to a triple exponential decay. It was demonstrated that a useful figure of merit in order to compare the relative enhancement factors of NWs of the same dimensions and the same multipole order, but made of different material or placed in different dielectric environment, is given by the ratio $[(\varepsilon_0 - \varepsilon')/\varepsilon'']^2$.

Acknowledgment. We are happy to offer this contribution to celebrate Professor G. C. Schatz 60th birthday and wish him much more happiness. E.A.C. will always be grateful to George for giving him the opportunity, as a post doc, to get involved in the fascinating field of Plasmonics. The authors thank SECyT UNC, FONCyT, and Agencia Córdoba Ciencia for financial support. E.R.E. and E.M.P. also acknowledge CONICET for doctoral fellowships. The authors thank B. T. Draine and P. J. Flatau for use of their DDA code, DDSCAT 6.1.

Supporting Information Available: Vector plots of the projection of the near-field enhancement on planes perpendicular to the major axis of a Ag NW ($L = 480$ nm, $d = 40$ nm), in vacuum, when illuminated at $\lambda_{res} = 570$ nm. This material is available free of charge via the Internet at http://pubs.acs.org.

References and Notes

(1) Barnes, W. L.; Dereux, A.; Ebbesen, T. W. *Nature* **2003**, *424*, 824.
(2) Haynes, C. L.; McFarland, A. D.; Zhao, L.; Van Duyne, R. P.; Schatz, G. C.; Gunnarsson, L.; Prikulis, J.; Kasemo, B.; Käll, M. *J. Phys Chem. B* **2003**, *107*, 7337.
(3) Maier, S. A.; Kik, P. G.; Atwater, H. A.; Meltzer, S.; Harel, E.; Koel, B. E.; Requicha, A. A. G. *Nat. Mater.* **2003**, *2*, 229.
(4) Kottmann, J. P.; Martin, O. J. F.; Smith, D. R.; Schultz, S. *Phys. Rev. B* **2001**, *64*, 235402.
(5) Feng Hao, F.; Nordlander, P.; Burnett, M. T.; Maier, S. A. *Phys. Rev. B* **2007**, *76*, 245417.
(6) Le, F.; Lwin, N. Z.; Halas, N. J.; Nordlander, P. *Phys. Rev. B* **2007**, *76*, 165410.
(7) Willets, K. A.; Van Duyne, R. P. *Annu. Rev. Phys. Chem.* **2007**, *58*, 267.
(8) Girard, C.; Martin, O. J. F.; Dereux, A. *Phys. Rev. Lett.* **1995**, *75*, 3098.
(9) Lance, K. K.; Coronado, E. A.; Zhao, L. L.; Schatz, G. C. *J. Phys. Chem. B* **2006**, *107*, 668.
(10) Novotny, L.; Stranick, S. J. *Annu. Rev. Phys. Chem.* **2006**, *57*, 303.
(11) Lee, S. J.; Guan, Z.; Xu, H.; Moskovits, M. *J. Phys. Chem. C* **2007**, *111*, 17985.
(12) Van Duyne, R. P. *Science* **2004**, *306*, 985.
(13) Jiang, J.; Bosnick, K.; Maillard, M.; Brus, L. *J. Phys. Chem. B* **2003**, *107*, 9964.
(14) (a) Schatz, G. C.; Young, M. A.; Van Duyne, R. P. *Top. Appl. Phys.* **2006**, *103*, 19. (b) *Surface-Enhanced Raman Scattering−Physics and Applications*; Kneipp, K., Moskovits, M., Kneipp, H., Eds.; Springer Verlag: Berlin, Heidelberg, Germany, 2006.
(15) Le, F.; Brandl, D. W.; Urzhumov, Y. A.; Wang, H.; Kundu, J.; Halas, N. J.; Aizpurua, J.; Nordlander, P. *ACS Nano* **2008**, *2*, 707.
(16) Stiles, P. L.; Dieringer, J. A.; Shah, N. C.; Van Duyne, R. P. *Annu. Rev. Anal. Chem.* **2008**, *1*, 601.
(17) Steidtner, J.; Pettinger, B. *Phys. Rev. Lett.* **2008**, *100*, 236101.
(18) Watanabe, H.; Ishida, Y.; Hayazawa, N.; Inouye, Y.; Kawata, S. *Phys. Rev. B* **2004**, *69*, 155418.
(19) Zhang, W.; Cui, X.; Yeo, B. S.; Schmid, T.; Hafner, C.; Zenobi, R. *Nano Lett.* **2008**, *7*, 1401.
(20) Zhang, W.; Yeo, B. S.; Schmid, T.; Zenobi, R. *J. Phys. Chem. C* **2007**, *111*, 1733.
(21) Becker, M.; Sivakov, V.; Andra, G.; Geiger, R.; Schreiber, J.; Hoffmann, S.; Michler, J.; Milenin, A. P.; Werner, P.; Christiansen, S. H. *Nano Lett.* **2007**, *7*, 75.
(22) Pettinger, B. *Top. Appl. Phys* **2006**, *103*, 217.
(23) Aslan, K.; Lakowicz, J. R.; Geddes, C. D. *Anal. Bioanal. Chem.* **2005**, *382*, 926.
(24) Stranik, O.; Nooney, R.; McDonagh, C.; MacCraith, B. D. *Plasmonics* **2007**, *2*, 15.
(25) Chowdhury, M. H.; Ray, K.; Aslan, K.; Lakowicz, J. R.; Geddes, C. D. *J. Phys. Chem. C* **2007**, *111*, 18856.
(26) Anger, P.; Bharadwaj, P.; Novotny, L. *Phys. Rev. Lett.* **2006**, *96*, 113002.
(27) Nie, S.; Emory, S. R. *Science* **1997**, *275*, 1102.
(28) Kneipp, K.; Wang, Y.; Kneipp, H.; Perelman, H. T.; Itzkan, I.; Dasari, R. R.; Feld, M. S. *Phys. Rev. Lett.* **1997**, *78*, 1667.
(29) Kneipp, K.; Kneipp, H.; Itzkan, I.; Dasari, R. R.; Feld, M. S. *Chem. Rev.* **1999**, *99*, 2957.
(30) Whitney, A. L.; Elam, J. W.; Zou, S.; Zinovev, A. V.; Stair, P. C.; Schatz, G. C.; Van Duyne, R. P. *J. Phys. Chem. B* **2005**, *109*, 20522.
(31) Haes, A. J.; Chang, L.; Klein, W. L.; Van Duyne, R. P. *J. Am. Chem. Soc.* **2005**, *127*, 2264.
(32) De Angelis, F.; Patrini, M.; Das, G.; Maksymov, I.; Galli, M.; Businaro, L.; Andreani, L. C.; Di Fabrizio, E. *Nano Lett.* **2008**, *8*, 2321.
(33) Anker, J. N.; Hall, W. P.; Lyandres, O.; Shah, N. C.; Zhao, J.; Van Duyne, R. P. *Nat. Mater.* **2008**, *7*, 442.
(34) Sriturayanich, W. W.; Fang, N.; Sun, C.; Luo, Q.; Zhang, X. *Nano Lett.* **2004**, *4*, 1085.
(35) Novotny L.; Hecht, B. *Principles of Nano-Optics*; Cambridge University Press: Cambridge, U.K., 2006.
(36) Novotny, L.; Stranick, S. J. *Annu. Rev. Phys. Chem.* **2006**, *57*, 303.
(37) Nelayah, J.; Kociak, M.; Stéphan, O.; García de Abajo, F. J.; Tencé, M.; Henrard, L.; Taverna, D.; Patoriza-Santos, I.; Liz-Marzán, L. M.; Colliex, C. *Nat. Phys.* **2007**, *3*, 348.
(38) Schider, G.; Krenn, J. R.; Ditlbacher, H.; Leitner, A.; Aussenegg, F. R.; Schaich, W. L.; Puscasu, I.; Monacelli, B.; Boreman, G. *Phys. Rev. B* **2003**, *68*, 155427.
(39) Laurent, G.; Felidj, N.; Aubard, J.; Levi, G.; Krenn, J. R.; Hohenau, A.; Schider, G.; Leitner, A.; Aussenegg, F. R. *Phys. Rev. B* **2005**, *71*, 45430.
(40) Payne, E. K.; Shuford, K. L.; Park, S.; Schatz, G. C.; Mirkin, C. A. *J. Phys. Chem. B* **2006**, *110*, 2150.
(41) Khlebtsov, B. N.; Khlebtsov, N. G. *J. Phys. Chem. C* **2007**, *111*, 11516.
(42) Encina, E. R.; Coronado, E. A. *J. Phys. Chem. C* **2007**, *111*, 16801.
(43) Encina, E. R.; Coronado, E. A. *J. Phys. Chem. C* **2008**, *112*, 9586.
(44) Ditlbacher, H.; Hohenau, A.; Wagner, D.; Kreibig, U.; Rogers, M.; Hofer, F.; Aussenegg, F. R.; Krenn, J. R. *Phys. Rev. Lett.* **2005**, *95*, 257403.
(45) Imura, K.; Nagahara, T.; Okamoto, H. *J. Chem. Phys.* **2005**, *122*, 154701.
(46) Imura, K.; Nagahara, T.; Okamoto, H. *J. Am. Chem. Soc.* **2004**, *126*, 12730.
(47) Vesseur, E. J. R.; de Waele, R.; Kuttge, M.; Polman, A. *Nano Lett.* **2007**, *7*, 2843.
(48) Ono, A.; Kato, J.; Kawata, S. *Phys. Rev. Lett.* **2005**, *95*, 267407.

(49) Xu, H.; Aizpurua, J.; Kall, M.; Apell, P. *Phys. Rev. E* **2000**, *62*, 4318.
(50) Purcell, E. M.; Pennypacker, C. R. *Astrophys. J.* **1973**, *186*, 705.
(51) Draine, B. T. *Astrophys. J.* **1988**, *333*, 848.
(52) *Handbook of Optical Constant of Solids*; Palik, E. D., Ed.; Academic Press: New York, 1985.
(53) Aizpurua, J.; Bryant, G. W.; Richter, L. J.; García de Abajo, F. J. *Phys. Rev. B* **2005**, *71*, 235.
(54) Bryant, G. W.; García de Abajo, F.; Aizpurua, J. *Nano Lett.* **2008**, *8*, 631.
(55) Novonty, L. *Phys. Rev. Lett.* **2007**, *98*, 266802.
(56) Schatz, G. C.; Van Duyne, R. P. In *Handbook of Vibrational Spectroscopy*; Chalmers, J. M., Griffiths, P., Eds.; Wiley: Chichester, U.K., 2002.
(57) Zeman, E. J.; Schatz, G. C. *J. Phys. Chem.* **1987**, *91*, 634.
(58) Xu, H.; Bjerneld, E. J.; Käll, M.; Börjesson, L. *Phys. Rev. Lett.* **1999**, *83*, 4357.

JP811089A